# Carbon isotope excursions during the late Miocene recorded by lipids of marine Thaumarchaeota, Piedmont Basin, Mediterranean Sea

Mathia Sabino, Daniel Birgel, Marcello Natalicchio, Francesco Dela Pierre, Jörn Peckmann

Supplemental Material

## The Messinian Sediments Of The Piedmont Basin

The studied sections are located in the proximal (Pollenzo) and distal (Govone) sectors of the southern margin of the Piedmont Basin (NW Italy), an Alpine retroforeland basin filled with Cenozoic sediments (Fig. S1; Dela Pierre et al., 2011; Sabino et al., 2020). The Messinian sediments are represented by outer shelf to upper slope shale/marl lithological cycles belonging to the Sant'Agata Fossili Marls Formation, testifying progressive basin restriction (Fig. S1; Dela Pierre et al., 2011). The lithological cyclicity reflects precession-paced climate fluctuations, with shales deposited under moister climate conditions (precession minima) and marls deposited under drier conditions (precession maxima; Natalicchio et al., 2019; Sabino et al., 2020). Starting from 5.97 Ma, shale/marl couplets make upslope transition to shale/gypsum lithological cycles, assigned to the Primary Lower Gypsum unit (Fig. S1; Dela Pierre et al., 2011). The lithological cyclicity of the unit, deposited during the first stage of the Messinian salinity crisis (MSC; 5.97 – 5.60 Ma; Roveri et al., 2014), was attributed to precession-driven climate fluctuations as well, with gypsum corresponding to precession maxima and arid conditions (Krijgsman et al., 1999). In deeper-water settings (> 200 m), gypsum deposition was delayed, possibly because of sulfate consumption driven by intense bacterial sulfate reduction favored by pronounced water-column stratification after the MSC onset (Fig. S1; de Lange and Krijgsman, 2010; Sabino et al., 2021). The Messinian succession of the Piedmont Basin terminates with resedimented evaporites and fluvio-deltaic deposits, representing the acme (5.60 – 5.55 Ma) and the final stage (5.55 – 5.33 Ma) of the MSC, respectively (Fig. S1; Dela Pierre et al., 2011).

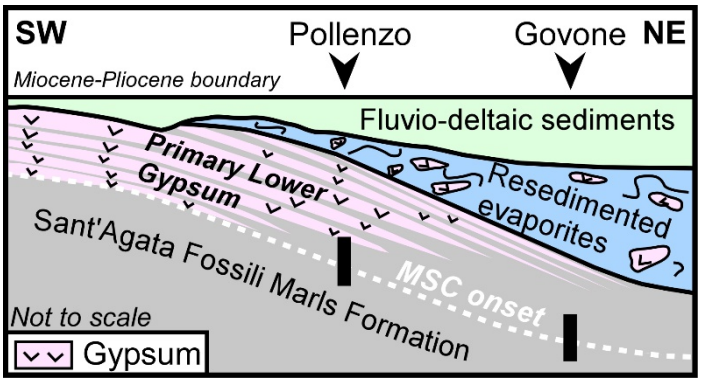


Figure S1. Schematic cross section of the Piedmont Basin showing the Messinian stratigraphy (modified from Sabino et al., 2021). The thick black bars indicate the investigated stratigraphic intervals of the proximal Pollenzo and distal Govone sections. MSC: Messinian salinity crisis.

## Lipid Biomarker Analyses

### Total Lipid Extracts (TLEs)

Lipid biomarkers were extracted applying the procedure described in detail in Sabino et al. (2020). After basic hydrolysis with 6% KOH in methanol (MeOH), the samples were repeatedly extracted through ultrasonication with dichloromethane (DCM)/MeOH (3:1, *v/v*) until the organic solvent phase became colorless. The basic hydrolysis products and the extracts were combined and the solution was

acidified with 10% HCl to a pH 2 for transferring also liberated fatty acids to the organic solvent phase. The latter, containing the extracted lipids, was evaporated and separated into an *n*-hexane-soluble fraction and a DCM-soluble fraction.

**High Pressure Liquid Chromatography (HPLC)-Mass Spectrometry (MS) – Analyses Of Glycerol Tetraether Lipids**

10% vol. of 57 total lipid extracts (TLE) from a sub-set of samples from Natalicchio et al. (2019; Pollenzo: 43 samples) and Sabino et al. (2021; Govone: 14 samples) was used to obtain isoprenoid and branched glycerol dialkyl glycerol tetraethers (*i*GDGTs and *b*GDGTs; Fig. S2) according to the method reported in Sabino et al. (2021). Briefly, after dissolution in *n*-hexane, an internal standard ($C_{46}$ GDGT; 12 mg/L) was added and 10 µL for each sample were analyzed using a Varian MS Workstation 6.91 HPLC system coupled to a Varian 1200L triple quadrupole mass spectrometer. Compound separation was achieved with a Grace Prevail Cyano column (150 mm × 2.1 mm; 3 µm particle size) and a guard column, held at 30 °C. The solvent gradient program was: linear change from 97.5% A (100% *n*-hexane) and 2.5% B (90% *n*-hexane: 10% 2-propanol; *v/v*) to 75% A and 25% B from 0 to 35 min; then linearly to 100% B in 5 min and held for 8 min. Thereafter, back to 97.5% A and 2.5% B to re-equilibrate the column for 12 min. Solvent flow (0.3 mL/min) was kept constant during the entire run time (60 min). The mass spectrometer was equipped with an atmospheric pressure chemical ionization (APCI) interface operated in positive ion mode was used for GDGTs identification. The APCI parameters were: $N_2$ as nebulizing gas with a pressure of 60 psi; temperature fluctuating between 35 °C and 40 °C, 50 °C as API housing temperature, 200 °C for the drying gas of the API, with a pressure of 12 psi; the APCI auxiliary gas temperature was 400 °C, and its pressure was 18 psi. The scanned spectral range was set at *m/z* 950 to 1500. Lipid abundances (Tab. S1, S2) were determined selecting base peaks (*m/z)* of *i*GDGTs, including ions symmetrically with ± 1.0 of target *m/z*.

**Ether Cleavage And Gas Chromatography-Mass Spectrometry (GC-MS)**

For the analyses of biphytanes (Fig. S2), *i*GDGTs (Pollenzo: 27 samples; Govone 14 samples) were subjected to ether cleavage following the procedure in Birgel et al. (2014). Briefly, polar compounds were isolated through liquid chromatography from 10% vol. of the TLE, after eluting hydrocarbons. The polar fraction was reacted for 4 h at 110 °C with HI and glacial $MeCO_2H$, 500 µl each. Excess $I_2$ was removed with 1 mL aqueous 5% $Na_2S_2O_3$ and the alkyl iodides were reduced to hydrocarbons with $LiAlH_4$ in 2 mL tetrahydrofuran (THF) for 3h at 110 °C under an Ar atmosphere. The THF was collected and $H_2O$ was added to completely deactivate excess $LiAlH_4$. The samples were dried with $Na_2SO_4$ and the solvent evaporated. Biphytanes were identified through comparison of retention times and published mass spectral data (Schouten et al., 1998a) after analyses with GC-MS systems at the University of Hamburg and the University of Vienna (samples in italics in Tab. S3). The system at the University of Hamburg consisted of a Thermo Scientific Trace GC Ultra coupled to a Thermo Scientific DSQ II mass spectrometer equipped with an Agilent HP-5MS UI fused silica column with a length of 30 m, a diameter of 0.25 mm, and a film thickness of 0.25 µm. The carrier gas was helium and the GC temperature program was: 50 °C (3 min); from 50 °C to 230 °C (held 2 min) at 25 °C/min; from 230 °C to 320 °C (held 20 min) at 6 °C/min. The system at the University of Vienna consisted of an Agilent 7890 A GC coupled to an Agilent 5975C inert MSD mass spectrometer equipped with an Agilent HP-5MS UI fused silica column analogous to the column described above. The carrier gas was helium and the GC temperature program was: 60°C (1 min) to 150°C at 10°C/min, then to 320°C (held 25 min) at 4°C/min.

## Desulfurization

Desulfurization was performed for the dichloromethane-soluble fractions (asphaltenes), according to the procedure described in Sabino et al. (2021). Briefly, after dissolving asphaltenes in 8 mL THF/ MeOH (1:1, *v/v*), 200 mg each of anhydrous $NiCl_2$ and $NaBH_4$ were added and left react for 1 h. The samples were centrifuged, the supernatant collected, and the solid residue extracted twice with DCM/ MeOH (1:1, *v/v*), combining the new supernatants with the initial extract. An aqueous solution was added to separate and collect the organic layer. Excess solvents were eliminated through a rotary evaporator and the residual organic phase was filtered through dry $NaSO_4$ to remove water. Hydrocarbons released after desulfurization were collected through column chromatography using *n*-hexane/DCM (9:1, *v/v*) as eluent and silica gel as stationary phase. Hydrocarbons, dissolved in *n*-hexane, were analyzed by using the GC-MS system from the University of Hamburg (see above) and the following GC temperature program: from 60 °C (1 min) to 150 °C at 15 °C/min and then up to 320 °C (held 40 min) at 4 °C/min. Compound identification was achieved through comparison of retention times and published mass spectral data, with a focus on $C_{27}$ to $C_{29}$ steranes and phytane (Fig. S2).

## Compound Specific $\delta^{13}C$ Values

Compound specific $\delta^{13}C$ values were determined, when possible, on ether cleaved acyclic and cyclic biphytanes, and phytane and $C_{27}$ to $C_{29}$ steranes released after desulfurization (Tab. S3, S4). Measurements (41 samples in total) were conducted at the University of Hamburg and the University of Vienna (in italics in Tab. S3, S4). $\delta^{13}C$ values are reported in ‰ versus the Vienna Pee Dee Belemnite (V-PDB) standard. Measurements at the University of Hamburg were performed using an Agilent 6890 GC, equipped with an Agilent HP-5MS UI fused silica column (length: 30 m × 0.25 mm i.d.; 0.25 µm film thickness) coupled via a Thermo Finnigan Combustion III to a Thermo Finnigan Delta Plus XL isotope mass spectrometer (GC-IRMS). The following temperature program was applied: 50 °C held for 2 at min, heating up to 320 °C with a rate of 12 °C/min and held for 35 min. An externally calibrated standard mixture of 15 *n*-alkanes ($C_{16}$ to $C_{30}$) with known isotopic composition was measured after every three to four samples to check for instrument precision. When possible, analyses were conducted at least in duplicates; the average analytical standard deviation was 0.4‰. Analyses at the University of Vienna (Department of Terrestrial Ecosystem Research) were performed using a Thermo Fisher Trace GC Ultra connected via a Thermo Fisher GC Isolink interface to a Thermo Fisher Delta V Advantage mass spectrometer. The GC system was equipped with the same column described above and the carrier gas was helium. The GC temperature program was: from 60 °C (1 min) to 150 °C at 10 °C/min and then up to 320 °C (held 25 min) at 4 °C/min. After 5 samples, an externally calibrated standard mixture of 25 *n*-alkanes ($C_{14}$ to $C_{38}$) with known isotopic composition was measured to check instrument precision. When possible, samples were measured at least in duplicate; the average analytical standard deviation was 0.3‰.

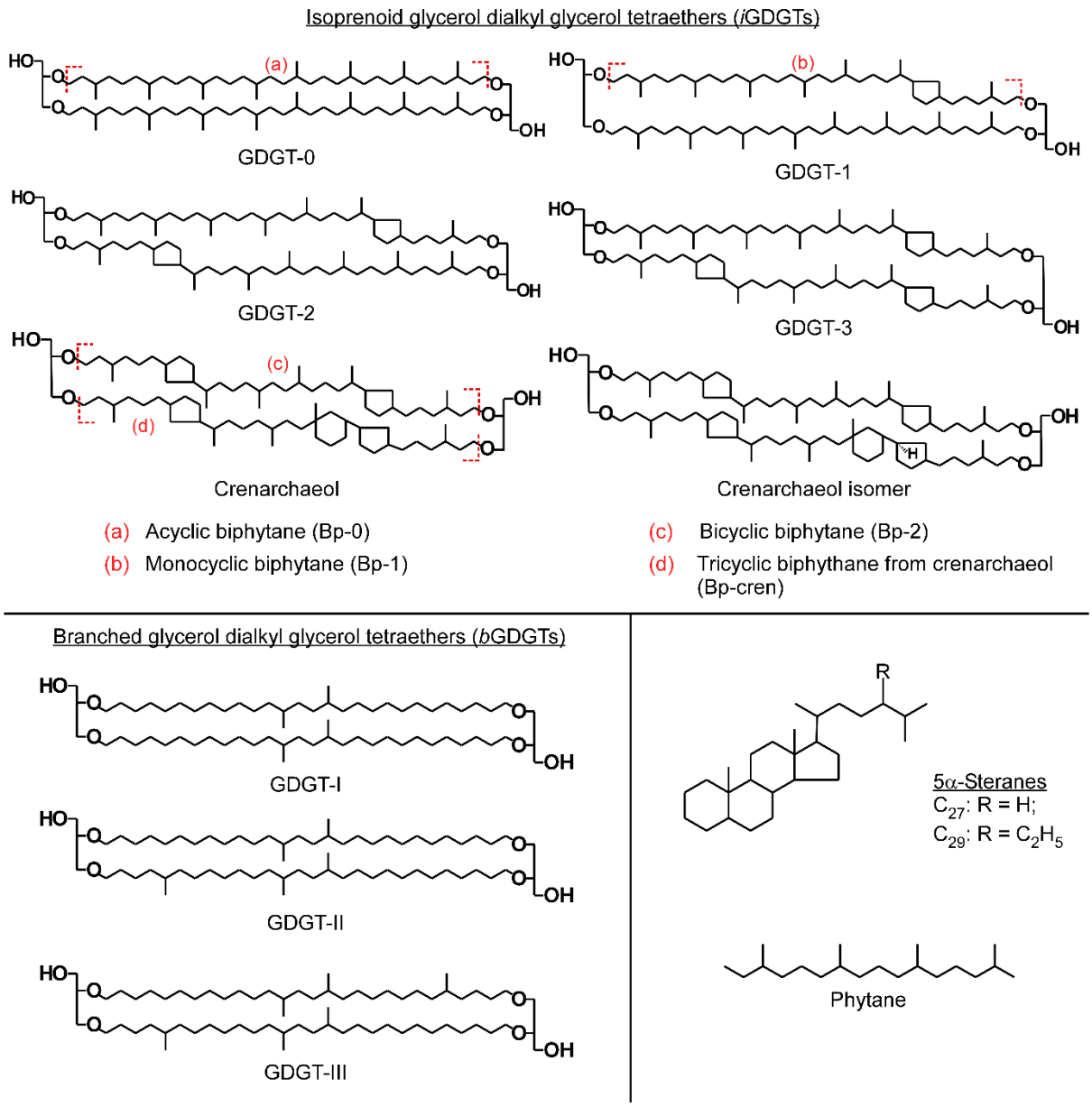


Figure S2. Structure of analyzed lipid biomarkers. Note in the structure of the crenarchaeol isomer the *cis* configuration of the cyclopentane ring adjacent to the cyclohexane ring according to Sinninghe Damsté et al. (2018).

Table S1. Abundance of isoprenoid glycerol dialkyl glycerol tetraethers (*i*GDGTs). Cren.: crenarchaeol; Cren'.: crenarchaeol isomer. [2]/[3]: *i*GDGT-2/*i*GDGT-3.

| Samples | *i* GDGTs (μg/g TOC) | | | | | | [2]/[3] ratio |
|---|---|---|---|---|---|---|---|
| | [0] | [1] | [2] | [3] | Cren. | Cren'. | |
| *Pollenzo section* | | | | | | | |
| Pg1.2.2 | 50.0 | 6.0 | 0.8 | - | 0.3 | - | - |
| Pg1_2.1 | 4.4 | 4.0 | 2.8 | 2.0 | 6.0 | 0.7 | 1.4 |
| Pg1_1.5 | 15.7 | 3.5 | 2.8 | 1.9 | 6.4 | 0.8 | 1.5 |
| Pg1_1.4 | 9.0 | 2.4 | 2.2 | 1.3 | 5.2 | 0.8 | 1.7 |
| Pg1.1.2 | 50.9 | 11.4 | 20.6 | 4.7 | 29.0 | 5.3 | 4.3 |
| Pg1_1.1 | 38.9 | 10.4 | 13.0 | 2.8 | 21.7 | 3.8 | 4.6 |
| Pm7_6.4 | 14.5 | 1.7 | 2.4 | 0.4 | 5.7 | 0.3 | 6.4 |
| Pm7_6.2 | 9.1 | 0.2 | 0.2 | 0.1 | - | - | 2.5 |
| Pm7_6.1 | 5.7 | 0.8 | 0.4 | 0.3 | 1.0 | 0.1 | 1.2 |
| Pm7_5.1 | 17.1 | 4.4 | 3.3 | - | 9.5 | 1.2 | - |
| Pm7_4.1 | 18.0 | 7.2 | 4.9 | 3.3 | 10.0 | 1.4 | 1.5 |
| Pm7_3.3 | 21.6 | 4.3 | 8.2 | 4.1 | 21.4 | 4.9 | 2.0 |
| Pm7_3.2 | 19.0 | 8.2 | 11.8 | 2.3 | 21.8 | 1.0 | 5.2 |
| Pm7_3.1 | 25.0 | 3.9 | 4.0 | 1.1 | 8.6 | 0.7 | 3.6 |
| Pm7_2.1 | 55.8 | 11.7 | 18.5 | 4.4 | 35.1 | 4.9 | 4.2 |
| Pm7_1.2 | 77.3 | 14.7 | 20.6 | 6.2 | 42.2 | 7.8 | 3.3 |
| Pm7_1.1 | 20.2 | 4.9 | 6.6 | 1.8 | 14.8 | 2.3 | 3.6 |
| Pm6_8.1 | 34.5 | 6.7 | 5.9 | 2.0 | 12.9 | 1.6 | 2.9 |
| Pm6_7.1 | 19.2 | 5.4 | 5.9 | 2.5 | 11.7 | 2.0 | 2.3 |
| Pm6_6.1 | 12.7 | 3.2 | 3.6 | 1.4 | 8.2 | 1.2 | 2.6 |
| Pm6_5.2 | 40.3 | 3.8 | 6.9 | 0.8 | 17.5 | 0.4 | 8.6 |
| Pm6_5.1 | 11.0 | 3.4 | 3.7 | 0.8 | 8.6 | 1.0 | 4.6 |
| Pm6_4.2 | 44.5 | 15.0 | 24.3 | 4.3 | 34.0 | 7.7 | 5.6 |
| Pm6_4.1 | 22.9 | 6.7 | 8.7 | 2.9 | 20.2 | 2.0 | 3.0 |
| Pm6_3.1 | 46.4 | 15.6 | 16.9 | 6.2 | 38.1 | 4.2 | 2.7 |
| Pm6_2.2 | 33.5 | 7.8 | 8.7 | 1.6 | 23.5 | 1.6 | 5.4 |
| Pm6_2.1 | 26.2 | 6.7 | 4.4 | 1.2 | 25.5 | 0.7 | 3.8 |
| Pm6_1.1 | 28.9 | 6.8 | 4.2 | 1.4 | 23.1 | 0.7 | 3.0 |
| Pm5_3.1 | 87.5 | 17.2 | 12.2 | 4.1 | 66.1 | 2.5 | 3.0 |
| Pm5_2.5 | 24.6 | 7.0 | 4.4 | 1.4 | 17.4 | 1.1 | 3.2 |
| Pm5_2.4 | 34.4 | 8.8 | 7.9 | 2.5 | 25.6 | 2.4 | 3.1 |
| Pm5_2.1 | 41.1 | 11.1 | 8.7 | 2.4 | 29.8 | 2.3 | 3.6 |
| Pm5_1.8 | 38.1 | 12.2 | 11.3 | 3.3 | 31.4 | 3.0 | 3.4 |
| Pm5_1.6 | 44.8 | 13.5 | 13.5 | 4.3 | 36.4 | 4.7 | 3.2 |
| Pm5_1.5 | 23.9 | 8.3 | 8.8 | 2.1 | 22.7 | 2.6 | 4.2 |
| Pm5_1.2 | 72.5 | 23.2 | 33.9 | 7.3 | 63.3 | 10.3 | 4.6 |
| Pm5_1.1 | 31.6 | 11.2 | 13.9 | 3.9 | 28.6 | 4.7 | 3.6 |
| Pm4_3.1 | 9.3 | 2.7 | 1.5 | 0.5 | 6.9 | 0.4 | 2.9 |
| Pm4_2.2 | 17.6 | 4.9 | 3.5 | 1.0 | 15.3 | 0.7 | 3.5 |
| Pm4_2.1 | 14.2 | 3.3 | 1.0 | - | 12.9 | 2.3 | - |
| Pm4_0.3 | 28.1 | 9.4 | 10.8 | 2.3 | 24.7 | 3.7 | 4.7 |
| Pm4_0.2 | 29.8 | 10.3 | 11.7 | 3.0 | 26.9 | 3.9 | 3.8 |
| Pm4_0.1 | 38.8 | 13.0 | 17.4 | 4.0 | 35.6 | 5.5 | 4.4 |

*[continuation of Tab. S1]*

| Samples | *i* GDGTs (µg/g TOC) | | | | | | [2]/[3] ratio |
|---|---|---|---|---|---|---|---|
| | [0] | [1] | [2] | [3] | Cren. | Cren'. | |
| *Govone section* | | | | | | | |
| Gm33.2 | 16.4 | 4.9 | 5.0 | 0.9 | 12.8 | 1.6 | 5.3 |
| Gm33.1 | 16.5 | 4.9 | 6.2 | 1.2 | 16.1 | 1.3 | 5.3 |
| Gm32.5 | 5.4 | 1.1 | 1.2 | 0.2 | 5.0 | 0.4 | 6.1 |
| Gm32.2 | 17.9 | 4.9 | 3.3 | 0.8 | 12.1 | 1.7 | 4.1 |
| Gm32.1 | 19.7 | 5.5 | 5.0 | 1.2 | 16.8 | 2.4 | 4.2 |
| Gm31.4 | 20.5 | 7.1 | 8.8 | 1.5 | 21.2 | 2.6 | 5.9 |
| Gm31.2 | 22.0 | 6.7 | 7.1 | 1.4 | 16.1 | 2.8 | 5.1 |
| Gm31.1 | 18.6 | 6.6 | 7.9 | 2.1 | 19.8 | 2.8 | 3.7 |
| Gm30.3 | 8.4 | 2.9 | 3.1 | 0.7 | 8.8 | 1.2 | 4.2 |
| Gm30.2 | 8.0 | 2.0 | 2.9 | 0.5 | 7.0 | 0.9 | 5.4 |
| Gm30.1 | 22.9 | 8.0 | 6.3 | 1.5 | 17.4 | 1.4 | 4.3 |
| Gm29.3 | 5.6 | 1.7 | 2.4 | 0.5 | 5.8 | 0.7 | 4.9 |
| Gm29.2 | 17.0 | 6.5 | 6.3 | 2.2 | 16.5 | 2.1 | 2.9 |
| Gm29.1 | 16.7 | 7.1 | 7.2 | 2.3 | 17.4 | 2.1 | 3.2 |

Table S2. Abundance of branched glycerol dialkyl glycerol tetraethers (*b*GDGTs). Branched and isoprenoid tetraether (BIT) index calculated according to Hopmans et al. (2004).

| Samples | *b* GDGTs (µg/g TOC) | | | BIT index | Samples | *b* GDGTs (µg/g TOC) | | | BIT index |
|---|---|---|---|---|---|---|---|---|---|
| | I | II | III | | | I | II | III | |
| *Pollenzo section* | | | | | *Pollenzo section* | | | | |
| Pg1.2.2 | 2.6 | 4.4 | 4.2 | 1.0 | Pm6_4.2 | 10.5 | 12.2 | 8.3 | 0.5 |
| Pg1_2.1 | 3.1 | 4.1 | 1.0 | 0.6 | Pm6_4.1 | 17.9 | 18.3 | 16.9 | 0.7 |
| Pg1_1.5 | 1.7 | 2.2 | 1.8 | 0.5 | Pm6_3.1 | 19.1 | 20.9 | 17.9 | 0.6 |
| Pg1_1.4 | 0.9 | 1.2 | 1.1 | 0.4 | Pm6_2.2 | 13.9 | 14.5 | 11.6 | 0.6 |
| Pg1.1.2 | 6.0 | 6.1 | 4.3 | 0.4 | Pm6_2.1 | 10.4 | 11.2 | 10.2 | 0.6 |
| Pg1_1.1 | 10.4 | 11.0 | 7.8 | 0.6 | Pm6_1.1 | 7.9 | 7.9 | 7.0 | 0.5 |
| Pm7_6.4 | 3.2 | 2.3 | 2.8 | 0.6 | Pm5_3.1 | 13.2 | 15.3 | 8.9 | 0.4 |
| Pm7_6.2 | 2.6 | 2.4 | 1.8 | 1.0 | Pm5_2.5 | 5.2 | 6.0 | 4.9 | 0.5 |
| Pm7_6.1 | 1.5 | 1.4 | 1.1 | 0.8 | Pm5_2.4 | 15.8 | 19.5 | 15.3 | 0.7 |
| Pm7_5.1 | 2.0 | 2.3 | 2.7 | 0.4 | Pm5_2.1 | 7.1 | 9.6 | 7.9 | 0.5 |
| Pm7_4.1 | 5.4 | 3.7 | 3.0 | 0.5 | Pm5_1.8 | 9.2 | 12.4 | 12.3 | 0.5 |
| Pm7_3.3 | 5.9 | 6.7 | 5.1 | 0.5 | Pm5_1.6 | 19.8 | 23.6 | 18.2 | 0.6 |
| Pm7_3.2 | 6.5 | 7.0 | 50.9 | 0.7 | Pm5_1.5 | 17.5 | 19.6 | 15.3 | 0.7 |
| Pm7_3.1 | 19.9 | 16.1 | 13.1 | 0.9 | Pm5_1.2 | 32.0 | 38.5 | 26.8 | 0.6 |
| Pm7_2.1 | 13.1 | 13.6 | 9.8 | 0.5 | Pm5_1.1 | 17.2 | 20.7 | 15.0 | 0.6 |
| Pm7_1.2 | 16.3 | 17.7 | 11.3 | 0.5 | Pm4_3.1 | 19.6 | 22.2 | 16.9 | 0.9 |
| Pm7_1.1 | 7.9 | 9.1 | 6.6 | 0.6 | Pm4_2.2 | 7.8 | 10.4 | 8.6 | 0.6 |
| Pm6_8.1 | 23.6 | 29.6 | 20.4 | 0.9 | Pm4_2.1 | 5.3 | 6.4 | 5.8 | 0.6 |
| Pm6_7.1 | 8.5 | 10.3 | 8.5 | 0.7 | Pm4_0.3 | 20.0 | 19.4 | 16.2 | 0.7 |
| Pm6_6.1 | 5.7 | 4.8 | 4.5 | 0.6 | Pm4_0.2 | 14.0 | 15.2 | 10.3 | 0.6 |
| Pm6_5.2 | 40.1 | 40.5 | 35.1 | 0.9 | Pm4_0.1 | 41.0 | 53.5 | 36.5 | 0.8 |
| Pm6_5.1 | 4.5 | 4.1 | 3.0 | 0.6 | | | | | |

*[continuation of Tab. S2]*

| Samples | *b* GDGTs (µg/g TOC) | | | BIT index | Samples | *b* GDGTs (µg/g TOC) | | | BIT index |
|---|---|---|---|---|---|---|---|---|---|
| | I | II | III | | | I | II | III | |
| *Govone section* | | | | | *Govone section* | | | | |
| Gm33.2 | 3.0 | 3.4 | 2.2 | 0.4 | Gm31.1 | 2.9 | 3.3 | 1.8 | 0.3 |
| Gm33.1 | 7.7 | 8.7 | 6.0 | 0.6 | Gm30.3 | 2.8 | 4.4 | 4.6 | 0.6 |
| Gm32.5 | 2.9 | 3.8 | 3.2 | 0.7 | Gm30.2 | 0.1 | 3.0 | 2.5 | 0.4 |
| Gm32.2 | 4.0 | 5.1 | 3.1 | 0.5 | Gm30.1 | 2.7 | 3.4 | 2.5 | 0.3 |
| Gm32.1 | 5.2 | 6.4 | 4.5 | 0.5 | Gm29.3 | 1.1 | 1.7 | 1.6 | 0.4 |
| Gm31.4 | 4.9 | 7.5 | 6.6 | 0.5 | Gm29.2 | 3.0 | 3.2 | 2.0 | 0.3 |
| Gm31.2 | 3.0 | 3.0 | 2.1 | 0.3 | Gm29.1 | 4.0 | 4.5 | 3.2 | 0.4 |

Table S3. Compound specific carbon stable isotopes ($\delta^{13}C$) of biphytanes (Bp) and Pearson correlation coefficient (r). SD: standard deviation; *: very low concentration and/or coelution; Bp-cren: tricyclic biphytane from crenarchaeol. Samples measured at the University of Vienna in italics.

| Samples | $\delta^{13}C_{Bp\text{-}0}$ (‰) | SD | $\delta^{13}C_{Bp\text{-}1}$ (‰) | SD | $\delta^{13}C_{Bp\text{-}2}$ (‰) | SD | $\delta^{13}C_{Bp\text{-}cren}$ (‰) | SD |
|---|---|---|---|---|---|---|---|---|
| *Pollenzo section* | | | | | | | | |
| Pg1_2.1 | -25.9 | 0.3 | -17.4 | 0.0 | -15.2 | 0.4 | -15.4 | 0.8 |
| Pg1_1.5 | -26.1 | 0.4 | -16.5 | 0.3 | -14.7 | 0.1 | -15.0 | 0.1 |
| Pg1_1.1 | -26.2 | 0.3 | -22.9 | 0.3 | -22.2 | 0.3 | -22.4 | 0.3 |
| Pm7_6.4 | -29.5 | 0.1 | -24.5 | 0.3 | -23.2 | 0.6 | -23.4* | 1.1 |
| Pm7_6.2 | -30.9 | 0.4 | - | - | - | - | - | - |
| *Pm7_6.1* | *-27.8* | *0.1* | - | - | *-18.3* | *0.6* | - | - |
| *Pm7_5.1* | *-24.2* | *0.4* | - | - | - | - | - | - |
| *Pm7_4.1* | *-25.4* | *0.5* | *-18.0* | *0.3* | *-16.9* | *0.4* | *-16.2* | *0.2* |
| Pm7_3.3 | -26.2 | 0.6 | -16.0 | 0.1 | -16.6 | 0.4 | -17.1 | 0.6 |
| Pm7_3.2 | -25.1 | 0.5 | -18.6 | 0.3 | -18.9 | 0.1 | -20.3 | 0.3 |
| Pm7_1.2 | -25.2 | 0.2 | -21.0 | 0.4 | -20.7 | 0.4 | -20.6 | 0.5 |
| *Pm6_8.1* | *-28.7* | *0.2* | *-23.4* | *0.3* | *-22.3* | *0.2* | *-21.4* | *0.2* |
| *Pm6_7.1* | *-24.7* | *0.2* | *-25.2* | *1.0* | *-16.1* | *1.8* | *-15.7** | *1.8* |
| *Pm6_6.1* | *-24.6* | - | *-17.1* | - | *-17.2* | - | *-17.1* | - |
| Pm6_5.1 | -26.4 | 0.2 | -23.8 | 0.9 | -23.4 | 0.5 | -23.3 | 0.3 |
| Pm6_4.1 | -26.5 | 0.2 | -23.9 | 0.1 | -22.4 | 0.2 | -23.2 | 0.0 |
| Pm6_2.1 | -21.0 | 0.3 | -17.1 | 0.2 | -17.5 | 0.4 | -17.1 | 0.3 |
| *Pm6_1.1* | *-21.3* | - | *-20.3* | - | *-19.4* | - | *-18.9* | - |
| *Pm5_3.1* | *-23.0* | *0.5* | *-20.3* | *0.0* | *-21.3* | *0.1* | *-20.7* | *0.0* |
| *Pm5_2.5* | *-23.1* | - | *-20.6* | - | *-21.1* | - | *-20.5* | - |
| Pm5_1.6 | -22.8 | 0.4 | -21.4 | 0.3 | -21.7 | 0.4 | -21.3 | 0.3 |
| Pm5_1.2 | -23.3 | 0.3 | -20.8 | 0.2 | -20.7 | 0.5 | -20.4 | 0.2 |
| *Pm4_3.1* | *-21.7* | *0.3* | *-21.5* | *0.8* | *-20.9* | *0.0* | *-20.9* | *0.1* |
| *Pm4_2.2* | *-20.1* | *0.1* | *-21.1* | *0.1* | *-18.5* | *0.1* | *-19.1* | *0.0* |
| *Pm4_2.1* | *-21.1* | *0.1* | *-20.3* | *0.0* | *-20.0* | *0.1* | *-20.0* | *0.1* |
| Pm4_0.3 | -25.4 | 0.0 | -23.8 | 0.1 | -22.8 | 0.1 | -22.8 | 0.1 |
| Pm4_0.2 | -22.8 | 0.9 | -21.8 | 0.9 | -21.3 | 0.4 | -21.2 | 0.1 |

*[continuation of Tab. S3]*

| Samples | $\delta^{13}C_{Bp-0}$ (‰) | SD | $\delta^{13}C_{Bp-1}$ (‰) | SD | $\delta^{13}C_{Bp-2}$ (‰) | SD | $\delta^{13}C_{Bp-cren}$ (‰) | SD |
|---|---|---|---|---|---|---|---|---|
| *Govone section* | | | | | | | | |
| Gm33.2 | -24.1 | 0.4 | -21.6 | 0.6 | -21.4 | 0.4 | -21.5 | 0.5 |
| Gm33.1 | -23.2 | 0.3 | -22.1 | 0.2 | -20.9 | 0.8 | -20.4 | 0.3 |
| Gm32.5 | -23.7 | 0.5 | -22.6 | 0.4 | -21.3 | 0.4 | -21.2 | 0.1 |
| Gm32.2 | -22.8 | 0.4 | -22.1 | 0.5 | -22.1 | 0.5 | -21.3 | 0.1 |
| Gm32.1 | -22.0 | 0.4 | -20.9 | 0.4 | -20.7 | 0.2 | -20.6 | 0.2 |
| Gm31.4 | -22.8 | 0.5 | -22.3 | 0.1 | -22.7 | 0.5 | -22.6 | 0.4 |
| Gm31.2 | -24.1 | 0.2 | -22.9 | 0.4 | -22.3 | 0.4 | -22.6 | 0.6 |
| Gm31.1 | -23.9 | 0.4 | -21.5 | 0.7 | -22.7 | 0.3 | -21.6 | 0.7 |
| Gm30.3 | -23.6 | 0.2 | -22.6 | 0.4 | -21.5 | 0.1 | -21.4 | 0.1 |
| Gm30.2 | -24.8 | 0.2 | -22.3 | 0.2 | -23.2 | 0.6 | -22.5 | 0.6 |
| Gm30.1 | -26.4 | 0.4 | -25.3 | 0.4 | -25.9 | 0.2 | -26.0 | 0.3 |
| Gm29.3 | -24.2 | 0.1 | -23.1 | 0.4 | -24.2 | 0.3 | -23.3 | 0.4 |
| Gm29.2 | -23.5 | 0.3 | -23.7 | 0.6 | -22.5 | 0.4 | -22.4 | 0.5 |
| Gm29.1 | -22.6 | 0.1 | -22.5 | 0.5 | -21.4 | 0.5 | -22.1 | 0.7 |

Pearson correlation coefficients (r) between $\delta^{13}C_{Bp-cren}$ and the other Bps

$r_{Bp-2} = 1.0$ $r_{Bp-1} = 0.8$ $r_{Bp-0} = 0.1$

Table S4. Compound specific carbon stable isotope values ($\delta^{13}C$) of lipids after desulfurization. Note that for the Govone section only the samples for which carbon stable isotope analyses were possible are reported (7 samples out of 14). Ph: phytane; SD: standard deviation.

| Samples | $\delta^{13}C$ phytane (‰) | SD | $\delta^{13}C$ 5α-$C_{27}$ sterane (‰) | SD | $\delta^{13}C$ 5α-$C_{29}$ sterane (‰) | SD |
|---|---|---|---|---|---|---|
| *Pollenzo section* | | | | | | |
| Pg1_1.5 | -26.0 | 0.0 | -23.9 | 0.3 | -23.7 | 0.3 |
| Pm7_4.1 | -24.4 | 0.4 | -24.3 | 0.1 | -25.6 | 0.1 |
| Pm6_7.1 | -24.8 | 0.0 | -23.5 | 0.3 | -24.9 | 0.0 |
| Pm6_5.1 | -27.4 | 0.1 | -25.7 | 0.3 | -26.5 | 0.2 |
| Pm6_1.1 | -22.4 | 0.2 | - | - | - | - |
| Pm5_1.6 | -27.7 | 0.5 | -26.5 | 0.8 | -27.6 | 0.9 |
| Pm4_3.1 | -27.9 | 0.8 | -26.3 | 0.1 | -25.2 | 0.7 |
| *Govone section* | | | | | | |
| Gm33.2 | -29.1 | 0.3 | -28.2 | 1.0 | -29.2 | 0.6 |
| Gm32.2 | -29.4 | 0.8 | -24.8 | 0.5 | -27.4 | 1.0 |
| Gm32.1 | -30.3 | 0.6 | -26.5 | 0.7 | -28.1 | 1.4 |
| Gm31.2 | -29.7 | 0.9 | -27.2 | 0.7 | -28.0 | 0.7 |
| Gm31.1 | -31.6 | - | -25.0 | 1.0 | -28.6 | 0.8 |
| Gm29.2 | -31.0 | - | -26.7 | 0.3 | -29.1 | 0.5 |
| Gm29.1 | -29.6 | 0.1 | -31.2 | 0.5 | -31.1 | 0.8 |

**Archaeal Sources of Acyclic, Monocyclic, And Bicyclic Biphytanes**

The $\delta^{13}C$ values of biphytanes (Bps) reported in Tab. S3 reveal that Bp-2 and Bp-cren show similar isotope composition for most samples, evidenced by the very high correlation between $\delta^{13}C_{Bp-cren}$ and $\delta^{13}C_{Bp-2}$ values. Therefore, Bp-2 has probably the same source as Bp-cren – crenarchaeol from marine group I (MGI) Thaumarchaeota. Accordingly, biases from $\delta^{13}C_{Bp-2}$ values by soil- or river-derived thaumarchaeal sources (GDGT-4 and crenarchaeol; see Sinninghe Damsté et al., 2012 for soil Thaumarchaeota) are negligible. This is further supported by the $^{13}C$ enrichment of Bp-2 with (1)

increasing BIT indices (Fig. S3A), and (2) increasing fluvial discharge after the MSC onset (cf. Natalicchio et al., 2019; Sabino et al., 2020), which is not expected in case of a major contribution from (1) soil Thaumarchaeota ($\delta^{13}C_{Bp\text{-}2} = -28.7 \pm 0.7$‰; Weijers et al., 2010) and (2) fluvial Thaumarchaeota (assuming a fractionation factor for the uptake of dissolved inorganic carbon (DIC) of about 20‰ [Könneke et al., 2012] and a $\delta^{13}C_{DIC}$ of −8‰ for fluvial waters [Marchina et al., 2016]), respectively. Conversely, a slight ($\delta^{13}C_{Bp\text{-}1}$) to moderate ($\delta^{13}C_{Bp\text{-}0}$) deviation relative to the $\delta^{13}C_{Bp\text{-}cren}$ (and $\delta^{13}C_{Bp\text{-}2}$) values was found (Tab. S3). The moderate correlation between $\delta^{13}C_{Bp\text{-}1}$ and $\delta^{13}C_{Bp\text{-}cren}$ values (Tab. S3) may suggest that MGI Thaumarchaeota are still the main source for Bp-1, although occasionally other sources must be considered. The very poor correlation between $\delta^{13}C_{Bp\text{-}0}$ and $\delta^{13}C_{Bp\text{-}cren}$ values strongly hint at a persistent additional source for Bp-0 (Tab. S3). Plotting the $\delta^{13}C_{Bp\text{-}0}$ and $\delta^{13}C_{Bp\text{-}1}$ values *vs.* the BIT index, a $^{13}C$ depletion in the $\delta^{13}C_{Bps}$ values is evident with increasing BIT indices, particularly for Bp-0 (Fig. S3B, C). Such a trend could suggest input from soil-derived methanogenic Euryarchaeota. In fact, Bp-0 and Bp-1 with $\delta^{13}C$ values ranging between −36‰ and −26‰ were reported from modern soils (Pancost et al., 2000; Pancost and Sinninghe Damsté, 2003; Oppermann et al., 2010; Weijers et al., 2010). However, a marked contribution exclusively from soil methanogenic Euryarchaeota seems unlikely considering that methanogenic Euryarchaeota are typically subordinated to Group I Thaumarchaeota in soils (Bates et al., 2011), whose input to the studied sediments was found to be negligible (see main text). According to the archaeal community reconstructed for the Piedmont Basin at the MSC onset, additional sources for Bp-1 and especially Bp-0 could alternatively be (1) sediment-dwelling methanogenic Euryarchaeota, and/or (2) heterotrophic planktonic marine Euryarchaeota (Natalicchio et al., 2017; Sabino et al., 2021). Possible input for cyclic *i*GDGTs (and hence Bp-1 to Bp-cren) from planktonic marine Euryarchaeota cannot be entirely excluded (e.g., Lincoln et al., 2014), although this possibility is still debated and controversial (Zeng et al., 2019; Besseling et al., 2020).

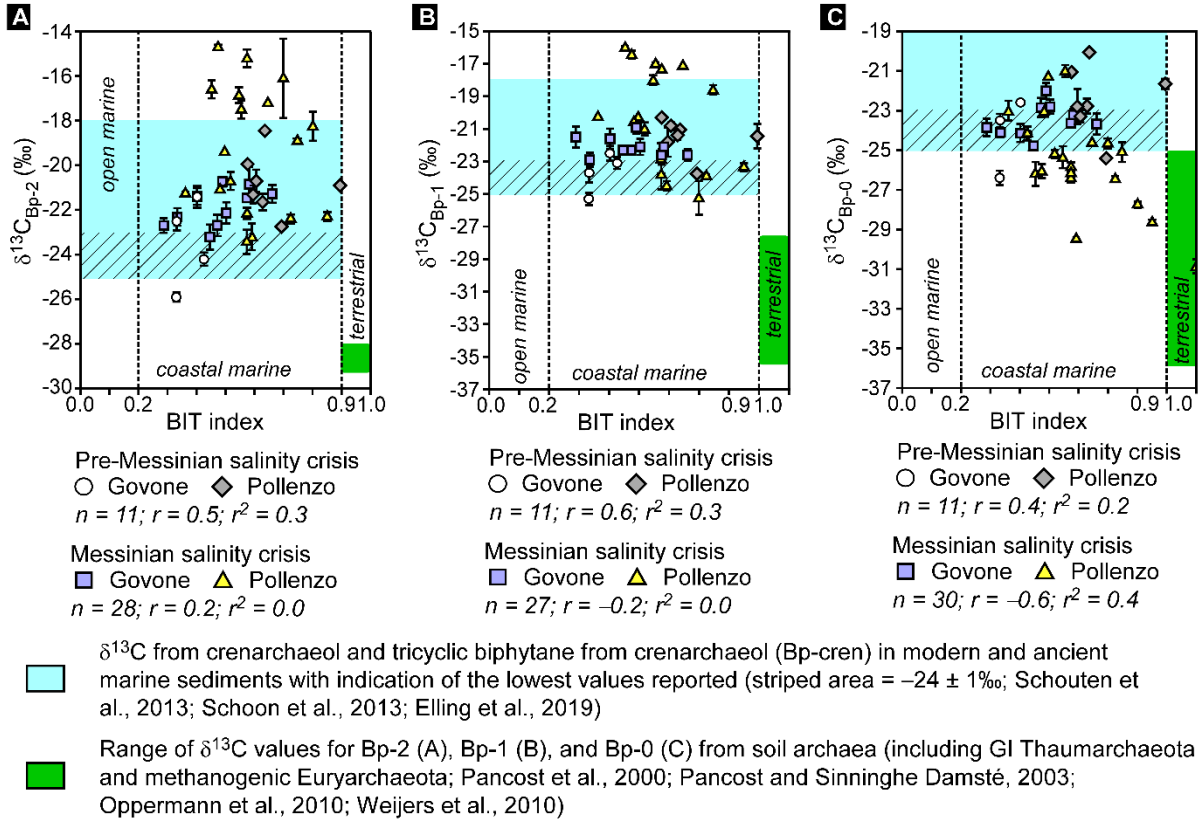


Figure S3. Branched and isoprenoid tetraether (BIT) index vs. the carbon stable isotope compositions of bicyclic ($\delta^{13}C_{Bp\text{-}2}$, A), monocyclic ($\delta^{13}C_{Bp\text{-}1}$, B), and acyclic ($\delta^{13}C_{Bp\text{-}0}$, C) biphytanes. GI: group I.

**Dominant Sources For Steranes And Phytane Released After Desulfurization**

Regular (5α) $C_{27}$ and $C_{29}$ steranes and phytane were released after desulfurization of asphaltenes from proximal (Pollenzo) and distal (Govone) sectors of the Piedmont Basin. Despite a relatively wide variability, the $\delta^{13}C$ values of the released steranes and phytane show overall $^{13}C$ enrichment toward younger samples and the highest values were almost exclusively recorded at the same stratigraphic level as observed for the lipids of MGI Thaumarchaeota from the more proximal parts of the Piedmont Basin (Tab. S3, S4). The common patterns suggest that the dominant source organisms of steranes and phytane were occupying the same environment as the MGI Thaumarchaeota community recording $^{13}C$ enrichment (cf. Schouten et al., 1998b), i.e. the upper water column (<200 m). Here, photosynthetic primary producers are the main source for steranes and phytane (e.g., Volkman, 2003; Knoll et al., 2007), whose respective $\delta^{13}C$ values can differ by as much as ±4-5‰ even when produced by the same organism (Schouten et al., 1998b). The difference between the $\delta^{13}C$ signature of steranes and phytane in almost all cases fall in this range and their $\delta^{13}C$ values co-vary. This observation supports a common source for phytane and $C_{27}$ and $C_{29}$ steranes released from desulfurization, i.e. algae dwelling in the upper water column.

**REFERENCES CITED**

Bates, S.T., Berg-Lyons, D., Caporaso, J.G., Walters, W.A., Knight, R., and Fierer, N., 2011, Examining the global distribution of dominant archaeal populations in soil: The ISME Journal, v. 5, p. 908–917, doi:10.1038/ismej.2010.171.

Besseling, M.A., Hopmans, E.C., Bale, N.J., Schouten, S., Sinninghe Damsté, J.S., and Villanueva, L.,

2020, The absence of intact polar lipid-derived GDGTs in marine waters dominated by Marine Group II: Implications for lipid biosynthesis in Archaea: Scientific Reports, v. 10, p. 1–10, doi:10.1038/s41598-019-57035-0.

Birgel, D., Guido, A., Liu, X., Hinrichs, K.-U., Gier, S., and Peckmann, J., 2014, Hypersaline conditions during deposition of the Calcare di Base revealed from archaeal di- and tetraether inventories: Organic Geochemistry, v. 77, p. 11–21, doi:10.1016/j.orggeochem.2014.09.002.

de Lange, G.J., and Krijgsman, W., 2010, Messinian salinity crisis: A novel unifying shallow gypsum/deep dolomite formation mechanism: Marine Geology, v. 275, p. 273–277, doi:10.1016/j.margeo.2010.05.003.

Dela Pierre, F. et al., 2011, The record of the Messinian salinity crisis in the Tertiary Piedmont Basin (NW Italy): The Alba section revisited: Palaeogeography, Palaeoclimatology, Palaeoecology, v. 310, p. 238–255, doi:10.1016/j.palaeo.2011.07.017.

Hopmans, E.C., Weijers, J.W.H., Schefuß, E., Herfort, L., Sinninghe Damsté, J.S., and Schouten, S., 2004, A novel proxy for terrestrial organic matter in sediments based on branched and isoprenoid tetraether lipids: Earth and Planetary Science Letters, v. 224, p. 107–116, doi:10.1016/j.epsl.2004.05.012.

Kim, J.H. et al., 2015, Influence of deep-water derived isoprenoid tetraether lipids on the $TEX_{86}^{H}$ paleothermometer in the Mediterranean Sea: Geochimica et Cosmochimica Acta, v. 150, p. 125–141, doi:10.1016/j.gca.2014.11.017.

Knoll, A.H., Summons, R.E., Waldbauer, J.R., and Zumberge, J.E., 2007, The geological succession of primary producers in the oceans *in* Falkowski, P.G., and Knoll, A.H., eds., Evolution of Primary Producers in the Sea: Elsevier Academic, Amsterdam, p. 133–163, doi:10.1016/B978-012370518-1/50009-6.

Könneke, M., Lipp, J.S., and Hinrichs, K.-U., 2012, Carbon isotope fractionation by the marine ammonia-oxidizing archaeon *Nitrosopumilus maritimus*: Organic Geochemistry, v. 48, p. 21–24, doi:10.1016/j.orggeochem.2012.04.007.

Krijgsman, W., Hilgen, F.J., Raffi, I., Sierro, F.J., and Wilson, D.S., 1999, Chronology, causes and progression of the Messinian salinity crisis: Nature, v. 400, p. 652–655, doi:10.1038/23231.

Lincoln, S.A., Wai, B., Eppley, J.M., Church, M.J., Summons, R.E., and DeLong, E.F., 2014, Planktonic Euryarchaeota are a significant source of archaeal tetraether lipids in the ocean: Proceedings of the National Academy of Sciences, v. 111, p. 9858–9863, doi:10.1073/pnas.1409439111.

Marchina, C., Bianchini, G., Knoeller, K., Natali, C., Pennisi, M., and Colombani, N., 2016, Natural and anthropogenic variations in the Po river waters (northern Italy): insights from a multi-isotope approach: Isotopes in Environmental and Health Studies, v. 52, p. 649–672, doi:10.1080/10256016.2016.1152965.

Natalicchio, M. et al., 2019, Paleoenvironmental change in a precession-paced succession across the onset of the Messinian salinity crisis: Insight from element geochemistry and molecular fossils: Palaeogeography, Palaeoclimatology, Palaeoecology, v. 518, p. 45–61, doi:10.1016/j.palaeo.2019.01.009.

Natalicchio, M., Birgel, D., Peckmann, J., Lozar, F., Carnevale, G., Liu, X., Hinrichs, K.-U., and Dela Pierre, F., 2017, An archaeal biomarker record of paleoenvironmental change across the onset of the Messinian salinity crisis in the absence of evaporites (Piedmont Basin, Italy): Organic Geochemistry, v. 113, p. 242–253, doi:10.1016/j.orggeochem.2017.08.014.

Oppermann, B.I., Michaelis, W., Blumenberg, M., Frerichs, J., Schulz, H.M., Schippers, A., Beaubien, S.E., and Krüger, M., 2010, Soil microbial community changes as a result of long-term exposure to a natural $CO_2$ vent: Geochimica et Cosmochimica Acta, v. 74, p. 2697–2716, doi:10.1016/j.gca.2010.02.006.

Pancost, R.D., van Geel, B., Baas, M., and Sinninghe Damsté, J.S., 2000, $\delta^{13}C$ values and radiocarbon

dates of microbial biomarkers as tracers for carbon recycling in peat deposits: Geology, v. 28, p. 663–666, doi:10.1130/0091-7613(2000)028<0663:CVARDO>2.3.CO;2.

Pancost, R.D., and Sinninghe Damsté, J.S., 2003, Carbon isotopic compositions of prokaryotic lipids as tracers of carbon cycling in diverse settings: Chemical Geology, v. 195, p. 29–58, doi:10.1016/S0009-2541(02)00387-X.

Roveri, M. et al., 2014, The Messinian Salinity Crisis: Past and future of a great challenge for marine sciences: Marine Geology, v. 352, p. 25–58, doi:10.1016/j.margeo.2014.02.002.

Sabino, M., Dela Pierre, F., Natalicchio, M., Birgel, D., Gier, S., and Peckmann, J., 2021, The response of water column and sedimentary environments to the advent of the Messinian salinity crisis: Insights from an onshore deep-water section (Govone, NW Italy): Geological Magazine, v. 158, p. 825–841, doi: 10.1017/ S0016756820000874.

Sabino, M., Schefuß, E., Natalicchio, M., Dela Pierre, F., Birgel, D., Bortels, D., Schnetger, B., and Peckmann, J., 2020, Climatic and hydrologic variability in the northern Mediterranean across the onset of the Messinian salinity crisis: Palaeogeography, Palaeoclimatology, Palaeoecology, v. 545, 109632, doi:10.1016/j.palaeo.2020.109632.

Schouten, S., Hoefs, M.J.L., Koopmans, M.P., Bosch, H.J., and Sinninghe Damsté, J.S., 1998a, Structural characterization, occurrence and fate of archaeal ether-bound acyclic and cyclic biphytanes and corresponding diols in sediments: Organic Geochemistry, v. 29, p. 1305–1319, doi:10.1016/S0146-6380(98)00131-4.

Schouten, S., Klein Breteler, W.C.M., Blokker, P., Schogt, N., Rijpstra, W.I.C., Grice, K., Baas, M., and Sinninghe Damsté, J.S., 1998b, Biosynthetic effects on the stable carbon isotopic compositions of algal lipids: implications for deciphering the carbon isotopic biomarker record: Geochimica et Cosmochimica Acta, v. 62, p. 1397–1406, doi:10.1016/S0016-7037(98)00076-3.

Sinninghe Damsté, J.S., Rijpstra, W.I.C., Hopmans, E.C., Jung, M.Y., Kim, J.G., Rhee, S.K., Stieglmeier, M., and Schleper, C., 2012, Intact polar and core glycerol dibiphytanyl glycerol tetraether lipids of group I.1a and I.1b Thaumarchaeota in soil: Applied and Environmental Microbiology, v. 78, p. 6866–6874, doi:10.1128/AEM.01681-12.

Sinninghe Damsté, J.S., Rijpstra, W.I.C., Hopmans, E.C., den Uijl, M.J., Weijers, J.W.H., and Schouten, S., 2018, The enigmatic structure of the crenarchaeol isomer: Organic Geochemistry, v. 124, p. 22–28, doi:10.1016/j.orggeochem.2018.06.005

Volkman, J.K., 2003, Sterols in microorganisms: Applied Microbiology and Biotechnology, v. 60, p. 495–506, doi:10.1007/s00253-002-1172-8.

Weijers, J.W.H., Wiesenberg, G.L.B., Bol, R., Hopmans, E.C., and Pancost, R.D., 2010, Carbon isotopic composition of branched tetraether membrane lipids in soils suggest a rapid turnover and a heterotrophic life style of their source organism(s): Biogeosciences, v. 7, p. 3691–3734, doi:10.5194/bgd-7-3691-2010.

Zeng, Z., Liu, X.-L., Farley, K.R., Wei, J.H., Metcalf, W.W., Summons, R.E., and Welander, P. V., 2019, GDGT cyclization proteins identify the dominant archaeal sources of tetraether lipids in the ocean: Proceedings of the National Academy of Sciences, v. 116, p. 22505–22511, doi:10.1073/pnas.1909306116.

Zhang, Y.G., Zhang, C.L., Liu, X.-L., Li, L., Hinrichs, K.-U., and Noakes, J.E., 2011, Methane Index: A tetraether archaeal lipid biomarker indicator for detecting the instability of marine gas hydrates: Earth and Planetary Science Letters, v. 307, p. 525–534, doi:10.1016/j.epsl.2011.05.031.